# 6.3. Modeling $N_2O$/NO formation and reduction during combustion of char

*Using the single particle model.*

*E.E. Beerling[a], G.Brem[b], E.A. Bramer[a], M. Valk[a].*

*[a] Department of Thermal Engineering, Twente University of Technology, P.O. Box 217, 7500 AE Enschede (The Netherlands)*

*[b] TNO-ME, P.O. Box 342, 7300 AH Apeldoorn (The Netherlands)*

## 6.3.1 INTRODUCTION

The method of combusting coal in a fluidized bed combustor has many advantages. Due to the low combustion temperature, the emission of $NO_x$ is low compared to conventional combustion techniques, because at these low temperatures the formation of $NO_x$ from $N_2$ and $O_2$ from the fluidizing air (thermal $NO_x$) and $NO_x$ formation through oxidation of char bound nitrogen (fuel $NO_x$), is less pronounced. Furthermore it is possible to reduce the emissions of $SO_2$ and $SO_3$ in the temperature range of a fluidized bed combustor by means of limestone addition to the bed.

A disadvantage of the low combustion temperature is that the emission of nitrous oxide ($N_2O$) is high compared to conventional combustion techniques. Nitrous oxide is a pollutant gas. It is a strong infrared absorber and therefore contributes to the greenhouse effect, causing global warming and it plays an important role in the depletion of the ozone layer.

The formation and reduction mechanisms of nitrous oxide during combustion of coal in a fluiduized bed combustor are very complex. A first distinction can be made between the nitrous oxide formation and reduction mechanisms during combustion of volatiles from the coal and the nitrous oxide formation and reduction mechanisms during combustion of char. The work reported in this paper is conducted to gain more inside in the $N_2O$ formation and reduction mechanisms in combination with NO formation and reduction mechanisms that are important during char combustion in a fluidized bed combustor. A first attempt is made to model the $N_2O$ and NO formation and reduction analytically by using the single particle model.

## 6.3.2 HETEROGENEOUS FORMATION AND REDUCTION MECHANISMS
*LITERATURE SURVEY*

In this section the results of a literature survey on nitrous oxide formation and reduction mechanisms are presented. Use has been made of the work done by Hulgaard [1] and Johnsson [2].

When a coal particle is introduced in a fluidized bed combustor it shall first experience a raise in temperature. Moisture absorbed in the coal particle shall evaporate. After this stage the volatiles from the coal start to evolve and volatile combustion begins. Once the volatiles are evolved a char particle remains. At this stage the char combustion begins. As stated earlier nitrous oxide can be formed and reduced during both volatile and char combustion. Fig. 6.3.1 shows a simplified reaction scheme for $N_2O$ formation and reduction during combustion of coal.

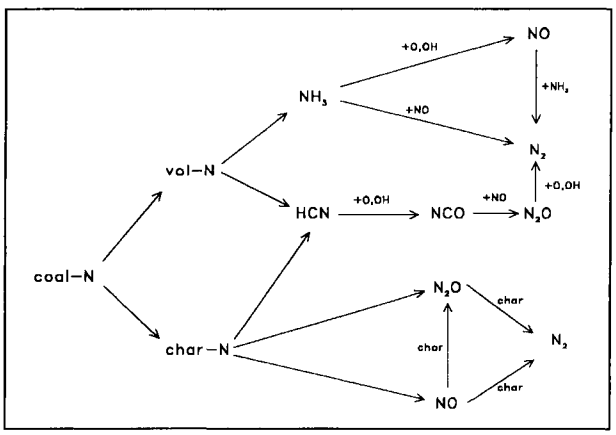


Figure 6.3.1. Simplified reaction scheme for nitrous oxide formation and reduction.

From literature it is clear that both volatile as char combustion play an important role in the $N_2O$ (and NO) reduction and formation. Valk and Bramer [5] found that char combustion was responsible for 1/3 of the total $N_2O$ produced. Wojtowicz et. al. [4] found that char combustion contributed 15 to 35 % (depending on the coal type used) to the total $N_2O$ production. The emphasis of this literature survey is on the nitrous oxide formation and reduction during char combustion. The reactions involved in the nitrous oxide formation and reduction are in this stage mainly heterogeneous solid-gas reactions.

### *6.3.2.1 Heterogeneous $N_2O$ formation*

De Soete [3] studied the formation of $N_2O$ by oxidation of char bound nitrogen using several types of char in a batchwise operated fixed-bed reactor. He found a

linear relationship between the $N_2O$ formation and the carbon conversion. The carbon conversion is defined as:

$$F_c = \int_0^t (X_{CO}+X_{CO_2})dt \Big/ \int_0^\infty (X_{CO}+X_{CO_2})dt \qquad (6.3.1)$$

where $X_i$ is the mole fraction of component i. He also found a linear relationship between the NO formation and the carbon conversion, as can be seen in Fig. 6.3.2.

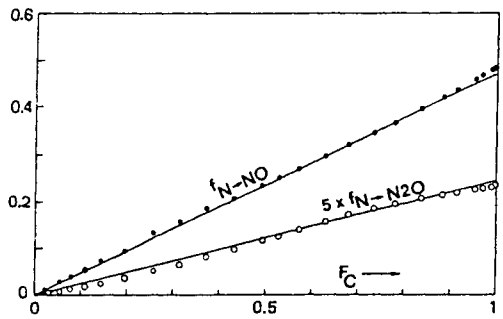


Figure 6.3.2. Conversion of char bound nitrogen to NO and $N_2O$. De Soete [3].

Fig. 6.3.2 depicts an overall effect. From the total amount of $N_2O$ produced by direct oxidation of char bound nitrogen, some $N_2O$ will be reduced on the char surface area. De Soete conducted his experiments at constant reactor temperature. So when assuming a first order behaviour for the $N_2O$ reduction reaction on the char surface area a linear relationship exists between the $N_2O$ formation by direct oxidation of char bound nitrogen and the carbon conversion . De Soete found that 1 to 6 percent of the char bound nitrogen was converted to $N_2O$ depending on the type of char used. Wojtowicz et.al. [4] report percentages between 2 and 10 percent. Bramer en Valk [5] found percentages between 1 and 1.6 percent. All the above mentioned researchers report a decrease in $N_2O$ emission with increasing reactor temperature.

Another possible mechanism of $N_2O$ formation mentioned in the literature is the formation of $N_2O$ caused by NO reduction on the char surface. De Soete [6] could not find significant $N_2O$ production from NO reduction in absence of oxygen. Bramer and Valk [5] used a micro-scale fluidized bed reactor to investigate this mechanism. They fed additional NO to the reactor operated under normal combustion conditions. The fuel used during these experiment was anthracite simulating char. Fig. 6.3.3 shows the results of these experiments.

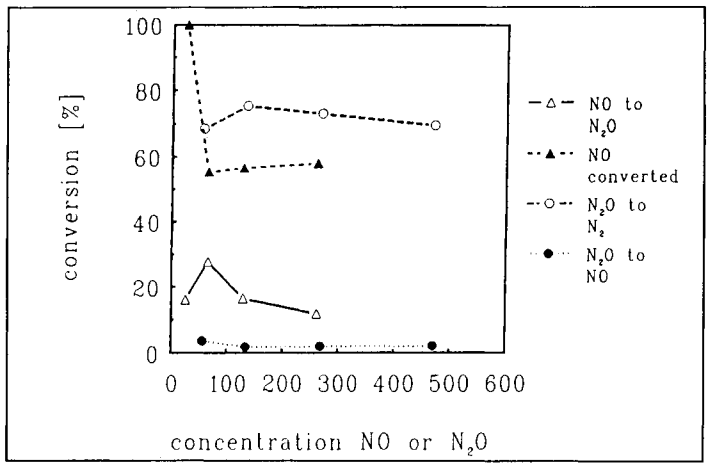


Figure 6.3.3. Conversion NO and $N_2O$ plotted against additional NO and $N_2O$ fed to the reactor. $T_{bed}$ = 1098 K, $\lambda = 1.2$, fuel = anthracite.
Bramer and Valk [5].

In fig. 6.3.3 several conversion factors are plotted against the concentration of the additional NO or $N_2O$ fed to the reactor. It can be seen that approximately 55 percent of the additional NO is reduced and that roughly 20 percent of last mentioned percentage is converted into $N_2O$. Amand et.al. [7] also found an increase in $N_2O$ emission when feeding NO to a fluidized bed reactor.

Another possible source of $N_2O$ is the formation of $N_2O$ by catalytic oxidation of $NH_3$. This $NH_3$ is a major reaction product during volatile combustion. Lisa et.al. [8] investigated the formation of $N_2O$ from $NH_3$ over CaO, $SiO_2$ and $CaSO_4$. CaO appeared to be the most effective catalyst for $N_2O$ formation when a mixture of $NH_3$ and $O_2$ was fed to the reactor. No $N_2O$ formation could be detected when $CaSO_4$ or $SiO_2$ was used as a catalyst.

From literature it appeares however that direct oxidation of char bound nitrogen is the major source of $N_2O$ during char combustion in a fluidized bed reactor.

### *6.3.2.2 Heterogeneous $N_2O$ reduction*

De Soete [9] investigated the decomposition of $N_2O$ on the char surface area. The main reaction products he found were $N_2$, HCN and NO. The amounts of NO and HCN appeared to be very small at temperatures below 1100 K. He also found a first order behaviour in $N_2O$ for this reduction reaction.

Santala et.al. [10] studied the $N_2O$ reduction on the surface areas of $SiO_2$, CaO and $CaSO_2$. Their experiments show that CaO is the most effective catalyst in reducing $N_2O$. $SiO_4$ (quartz sand) had only a little effect. The results are shown in fig. 6.3.4.

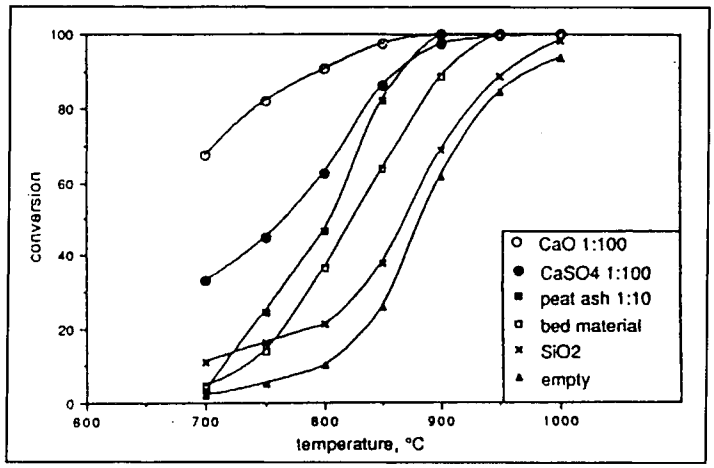


Figure 6.3.4. $N_2O$ conversion (%) as function of temperature on surface of amongst others CaO, $CaSO_4$, $SiO_2$ and bedmaterial in a coal fired fluidized bed combustor. The component is mixed with quartz sand in the ratio as listed in the figure. Santala [10].

Miettinen et.al. [11] also investigated the $N_2O$ reduction reaction and came to the same conclusions as Santala. So from literature it appeares that Ca containing components and char are effective catalysts in reducing $N_2O$. It also appeares that quartz sand has only a little effect on the $N_2O$ reduction.

## 6.3.3. MODELING

In this section a first attempt is made to model the $N_2O$ and NO reduction capacities of a single char particle analytically. The single particle model, proposed by Brem [12], will be used (see section 6.1). The reduction capacity is the ratio between the reduction and production rate of $N_2O$ (or NO).

### *6.3.3.1 The single particle model.*

In the single particle model some assumptions are made, described in section 6.1.2. The stoichiometric reaction coefficient in the combustion reaction is close to unity when combusting char under normal fluidized bed combustion. Furthermore isothermal conditions are presumed (bed and char particles have the same temperature.

*6.3.3.2 The $N_2O$ and NO reduction capacities.*

In this subsection the single particle model is used to derive the expressions for the $N_2O$ and NO reduction capacities under the assumption of a linear case, that is all reactions involved are first order reactions in the gaseous reactant, constant internal surface area of the char and constant effective diffusivity coefficient. The reduction capacity of a single char particle is defined as the ratio of the reduction rate and the formation rate, in formula (for the $N_2O$ reduction capacity):

$$R_{N_2O} = \frac{\int_0^{r_s} R_{N_2O,\,r}\, 4\pi r^2 dr}{\int_0^{r_s} R_{N_2O,\,f}\, 4\pi r^2 dr} \qquad (6.3.2)$$

In this formula $R_{N2O,\,r}$ is the $N_2O$ reduction rate and $R_{N2O,\,f}$ is the $N_2O$ formation rate.
The assumption is made that the major source of $N_2O$ is the oxidation of char bound nitrogen inside the particle. The thus formed $N_2O$ can be reduced on the char surface area on its way out of the particle. Depending on the value of the $N_2O$ reduction capacity it is also possible that $N_2O$ from the bulk is reduced on the char surface area.
First the expression for de $N_2O$ formation rate will be derived. The formation rate of $N_2O$ is assumed to be proportional to the char combustion rate. In formula:

$$R_{N_2O,f} = -\frac{\partial C_s}{\partial t} X_{NC}\, \gamma_{N_2O} \qquad (6.3.3)$$

with:

| | | |
|---|---|---|
| $C_s$ | = | carbon concentration in the particle |
| t | = | time |
| $X_{NC}$ | = | molar ratio of nitrogen and carbon in the char |
| $\gamma_{N2O}$ | = | molar ratio of the amount $N_2O$ formed by direct oxidation from the total amount of nitrogen in the char |

The mass balance of the solid reactant (carbon) can be written as:

$$\frac{\partial C_s}{\partial t} = -R_s \qquad (6.3.4)$$

with $R_s$ the reaction rate of carbon, in formula:

$$R_s = k_s \, C_{O_2} \, A_g \tag{6.3.5}$$

with: $k_s$ = reaction rate constant
$A_g$ = reaction surface area per unit of volume
$C_{O2}$ = local oxygen concentration

Using equation (6.3.4) and (6.3.5), equation (6.3.3) can be written as:

$$R_{N_2O,f} = k_s \, C_{O_2} \, A_g \, X_{NC} \, \gamma_{N_2O} \tag{6.3.6}$$

The assumption is made that $N_2O$ can only be reduced on the char surface area. In that case the $N_2O$ reduction rate can be written as follows:

$$R_{N_2O,r} = k_{N_2O} \, C_{N_2O} \, A_g \tag{6.3.7}$$

In latter formula $k_{N2O}$ is the reaction rate constant for the $N_2O$ reduction reaction.

*6.3.3.2.1 Mass balances.*

The pseudo-steady-state $N_2O$ mass balance can be written as follows:

$$\frac{1}{r^2} \frac{\partial}{\partial r} \left( D_e \, r^2 \, \frac{\partial C_{N_2O}}{\partial r} \right) + k_s \, C_{O_2} \, A_g \, X_{NC} \, \gamma_{N_2O} - k_{N_2O} \, C_{N_2O} \, A_g = 0 \tag{6.3.8}$$

where r is the radial coordinate and $D_e$ is the effective diffusivity. In formula (6.3.8) use has been made of formulas (6.3.6) and (6.3.7).

The boundary conditions are:

$$t = 0 \qquad C_{N_2O} = 0$$

$$r = 0 \qquad \frac{\partial C_{N_2O}}{\partial r} = 0$$

$$r = r_s \qquad D_e \frac{\partial C_{N_2O}}{\partial r} = k_d \left(C_{N_2O,\,\infty} - C_{N_2O,\,s}\right) \tag{6.3.9}$$

where $r_s$ is the particle radius, $k_d$ is the mass transfer coefficient in the external gas film, $C_{N2O,\,\infty}$ and $C_{N2O,\,s}$ are the $N_2O$ concentration in the bulk and the $N_2O$ concentration at the particle outer surface, respectively.

In order to solve equation (6.3.8) it is necessary to find an expression for the $O_2$ profile. The dimensionless oxygen mass balance can be written as follows:

$$\frac{2}{\zeta}\frac{\partial C}{\partial \zeta} + \frac{\partial^2 C}{\partial \zeta^2} - \Phi_o^2 C = 0 \tag{6.3.10}$$

with $\zeta = r/R$, $C = C_{O2}/C_{O2,\,\infty}$ and $\Phi_o$ is the Thiele modulus,

$$\Phi_o = R\sqrt{\frac{k_s A_g}{D_e}} \tag{6.3.11}$$

The dimensionless boundary conditions can be written as follows:

$$\theta = 0 \qquad C = 0$$

$$\zeta = 0 \qquad \frac{\partial C}{\partial \zeta} = 0$$

$$\zeta = \zeta_s \qquad D_e \frac{\partial C}{\partial \zeta} = Bi_m(1 - C_s) \tag{6.3.12}$$

where $\zeta_s = r_s/R$, $C_s$ is the reduced oxygen concentration at the external surface of the particle, $Bi_m$ is the Biot number for mass transfer defined as:

$$Bi_m = R \frac{k_d}{D_e} \tag{6.3.13}$$

$\theta$ is the reduced time defined as:

$$\theta = \frac{k_s C_{O_2,\infty} A_g t}{C_{s,o}} \tag{6.3.14}$$

where $C_{s,o}$ is the initial carbon concentration in the particle.

Equation (6.3.10) can now be solved which leads to the following expression for the reduced oxygen concentration in the particle:

$$C = \frac{Bi_m}{\frac{\sinh(\Phi_o \zeta_s)}{\zeta_s}(Bi_m + \Phi_o \coth(\Phi_o \zeta_s) - \frac{1}{\zeta_s})} \frac{\sinh(\Phi_o \zeta)}{\zeta} \tag{6.3.15}$$

Now the $N_2O$ mass balance can be solved. First equation (6.3.8) is written in the dimensionless form:

$$\frac{2}{\zeta}\frac{\partial N^*}{\partial \zeta} + \frac{\partial^2 N^*}{\partial \zeta^2} - \Phi_{N_2O}^2 N^* + \gamma_1 \Phi_o^2 C = 0 \tag{6.3.16}$$

where $N^* = C_{N2O}/C_{N2O,\infty}$, $\gamma_1 = \gamma_{N2O} X_{NC} C_{O2,\infty}/C_{N2O,\infty}$ and $\Phi_{N2O}$ the Thiele modulus defined as:

$$\Phi_{N_2O} = R \sqrt{\frac{k_{N_2O} A_g}{D_e}} \tag{6.3.17}$$

The reduced boundary conditions are:

$$\theta = 0 \qquad N^* = 0$$

$$\zeta = 0 \qquad \frac{\partial N^*}{\partial \zeta} = 0$$

$$\zeta = \zeta_s \qquad D_e \frac{\partial N^*}{\partial \zeta} = Bi_m(1 - N_s^*) \tag{6.3.18}$$

where $N_s^*$ is the reduced $N_2O$ concentration at the external surface of the particle. Equation (6.3.16) can now be solved which gives the following expression for the reduced $N_2O$ profile in the particle:

$$N^* = \frac{Bi_m\left(1 + \dfrac{\gamma_1}{1 - \Phi_{N_2O}^2/\Phi_o^2}\right)}{\dfrac{\sinh(\Phi_{N_2O}\zeta_s)}{\zeta_s}(Bi_m + \Phi_{N_2O}\coth(\Phi_{N_2O}\zeta_s) - \dfrac{1}{\zeta_s})} \frac{\sinh(\Phi_{N_2O}\zeta)}{\zeta} - \frac{\gamma_1}{1 - \Phi_{N_2O}^2/\Phi_o^2} C \tag{6.3.19}$$

where C is the dimensionless oxygen concentration described by equation (6.3.15).

With equations (6.3.15) and (6.3.19) the expression for the $N_2O$ reduction capacity can be derived. The definition of the $N_2O$ reduction capacity of formula (6.3.2) can be written in dimensionless form:

$$R_{N_2O} = \frac{1}{\gamma_1} \frac{\dfrac{\partial N^*}{\partial \zeta}\Big|_{\zeta_s}}{\dfrac{\partial C}{\partial \zeta}\Big|_{\zeta_s}} + 1 \tag{6.3.20}$$

Application of equations (6.3.15) and (6.3.19) in formula (6.3.20) results in the following expression for the $N_2O$ reduction capacity:

$$R_{N_2O} = 1 + \frac{1}{\gamma_1}\left[(C_1 - C_2) * C_3 - C_4\right] \qquad (6.3.21)$$

where:

$$C_1 = \frac{\Phi_{N_2O}\coth(\Phi_{N_2O}\zeta_s)Bi_m(1 + C_4)}{Bi_m + \Phi_{N_2O}\coth(\Phi_{N_2O}\zeta_s) - 1/\zeta_s}$$

$$C_2 = \frac{Bi_m(1 + C_4)}{[Bi_m + \Phi_{N_2O}\coth(\Phi_{N_2O}\zeta_s) - 1/\zeta_s]\zeta_s}$$

$$C_3 = \frac{1}{Bi_m} + \frac{\zeta_s}{\zeta_s\Phi_o\coth(\Phi_o\zeta_s) - 1}$$

$$C_4 = \frac{\gamma_1}{1 - \Phi_{N_2O}^2/\Phi_o^2}$$

The only unknown factor in the formula for the $N_2O$ reduction capacity is the reduced radius of the particle $\zeta_s$. Ishida and Wen [13] derived a relationship between the reduced particle radius and the conversion degree X for the linear case:

$$X = 1 - \zeta_s^3 + \frac{3\zeta_s}{\Phi_o^2}\left[\Phi_o\zeta_s\coth(\Phi_o\zeta_s) - 1\right] \qquad (6.3.22)$$

It can be shown that the $N_2O$ reduction capacity is only a weak function of the conversion degree X (and also of the reduced particle radius) except for conversion degrees close to unity. The assumption is made that a char particle in a fluidized bed reactor can not reach a conversion close to unity because at high conversion degrees the char particle becomes so small that it will be elutriated. In this case a constant value of unity will be adopted for the reduced particle radius $\zeta_s$ (i.e. the initial situation) in the expression for the $N_2O$ reduction capacity of a single particle. This adoption simplifies the expression for the $N_2O$ reduction capacity considerably:

$$R_{N_2O} = 1 + \frac{1}{\gamma_1}\left(\left[\frac{\left(1 + \frac{\gamma_1}{1 - \Phi_{N_2O}^2/\Phi_o^2}\right) Bi_m\,[\Phi_{N_2O}\coth(\Phi_{N_2O}) - 1]}{Bi_m + \Phi_{N_2O}\coth(\Phi_{N_2O}) - 1}\right] *\right.$$

$$\left.\left[\frac{1}{Bi_m} + \frac{1}{\Phi_o\coth(\Phi_o) - 1}\right] - \frac{\gamma_1}{1 - \Phi_{N_2O}^2/\Phi_o^2}\right) \qquad (6.3.23)$$

The same procedure as decribed above can be used to derive an expression for the NO reduction capacity of a single particle. The formation rate of NO is assumed to be proportional to the char combustion rate, in formula:

$$R_{NO,f} = -\frac{\partial C_s}{\partial t} X_{NC}\,\gamma_{NO} = k_s\,C_{O_2}\,A_g\,X_{NC}\,\gamma_{NO} \qquad (6.3.24)$$

where $\gamma_{NO}$ is the molar ratio of the amount NO formed by direct oxidation from the total amount of nitrogen in the char.

The assumption is made that NO can only be reduced on the char surface area. In that case the NO reduction rate can be written as follows:

$$R_{NO,r} = k_{NO}\,C_{NO}\,A_g \qquad (6.3.25)$$

Making use of equations (6.3.24) and (6.3.25), the NO reduction capacity can be written as:

$$R_{NO} = 1 + \frac{1}{\gamma_2}\left(\left[\frac{\left(1 + \frac{\gamma_2}{1 - \Phi_{NO}^2/\Phi_o^2}\right) Bi_m\,[\Phi_{NO}\coth(\Phi_{NO}) - 1]}{Bi_m + \Phi_{NO}\coth(\Phi_{NO}) - 1}\right] *\right.$$

$$\left.\left[\frac{1}{Bi_m} + \frac{1}{\Phi_o\coth(\Phi_o) - 1}\right] - \frac{\gamma_2}{1 - \Phi_{NO}^2/\Phi_o^2}\right) \qquad (6.3.26)$$

where:

$$\gamma_2 = X_{NC}\,\gamma_{NO}\,\frac{C_{O_2,\infty}}{C_{NO,\infty}} \tag{6.3.27}$$

$$\Phi_{NO} = R\sqrt{\frac{k_{NO}\,A_g}{D_e}} \tag{6.3.28}$$

## 6.3.4 MICRO-SCALE EXPERIMENTS

In order to investigate the $N_2O$ reduction and formation mechanisms during combustion of char, some micro-scale experiments have been conducted.

### *6.3.4.1 Experimental set-up.*

Figure 6.3.5 showes the experimental set-up used.

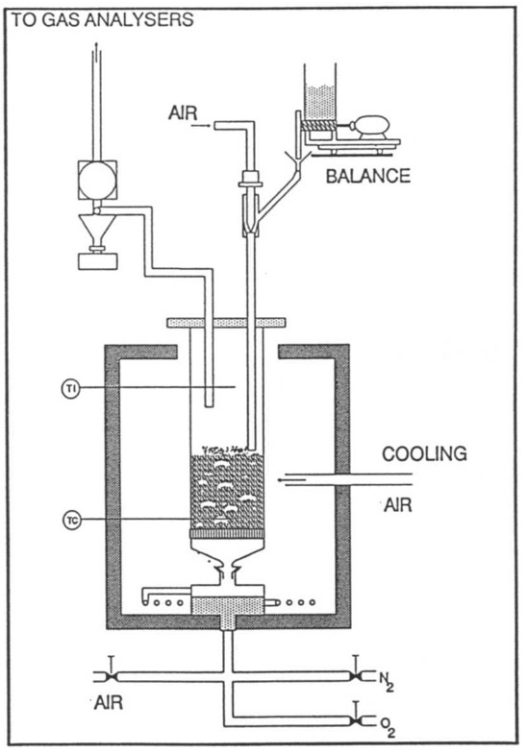


Figure 6.3.5. Experimental set-up.

The reactor is a ø 10 cm quartz tube with a porous quartz distributor plate. The height of the reactor is 65 cm. The reactor is situated in an electrically heated oven together with the gas preheater. The gas composition and the gas flow entering the reactor can be adjusted by means of critical flow nozzles. Char can continuously be supplied to the reactor (above the bed) by a small hopper and screw feeder with a variable speed motor. The whole feeding system is placed on a digital balance. The temperature of the oven is regulated by a temperature controller, the excess heat can be removed by cooling air around the reactor.

The effluent gases can be analysed by the following equipment:

- CO: Beckman model 870 (Non-dispersive infrared absorption, 0 - 5 vol %)
- CO: Maihak Defor (Non-dispersive infrared absorption, 0 - 0.5 vol %)
- CH: Beckman model 400 (Flame ionisation detection, 0 - 10000 ppmV)
- $NO/NO_x$: Beckman model 951 A (Chemiluminescention, 0 - 1000 ppmV)
- $SO_2$: Maihak Defor (Non-dispersive infrared absorption, 0 - 1000 ppmV)
- $O_2$: Maihak Oxigor 6N (Paramagnetic, 0 - 20 vol %)
- $CO_2$: Maihak Defor (Non-dispersive infrared absorption, 0 - 20 vol %)
- $N_2O$: Miran Infrared Analyser model 80 (Infrared absortion, range depending on calibration)

*6.3.4.2 Preparation of the char.*

The char used for the experiments was produced from El Cerrejon coal in a ø 30 cm fluidized bed reactor. The reactor was heated up to 880 °C. At this temperature 10 kg of coal (sieve fraction 2 - 6.3 mm) was supplied to the reactor. For 8 minutes the reactor was fired with petroleum under lean condition. Then the air supply to the reactor was stopped and the reactor was cooled down to 350 °C under an inert atmosphere. The analysis of the resulting char is shown in table 6.3.1.

Table 6.3.1. Analysis of the char.

| Char: El Cerrejon | | Land of origin: Columbia |
|---|---|---|
| ULTIMATE ANALYSIS | | WEIGHT PERCENTAGE |
| Carbon | C | 84.21 |
| Hydrogen | H | 0.54 |
| Oxygen | O | 3.12 |
| Nitrogen | N | 1.61 |
| Sulphur | S | 0.62 |
| Volatile matter | | 4.76 |
| Fixed carbon | | 85.35 |
| Moisture | | 2.09 |
| Ash | | 9.89 |

The density of the char $\rho_c$ is 750 kg/m$^3$, the bulk density $W_g$ is 335 kg/m$^3$ and the fixed-bed porosity $\epsilon$ (the ratio of the density of the char and the bulk density of the char) is 0.45. The value of the surface area of the char A is difficult to determin, so a value of 600 m$^2$/g is adopted from literature (van Engelen et.al. [14]).

*6.3.4.3 Experimental program*

Experiments have been conducted to gain more inside in the following subjects:

- Thermal $N_2O$ decomposition.
- $N_2O$ reduction reaction at the char surface area.
- $N_2O$ formation through NO reduction at the char surface area.
- Combustion (parametric study).

The experimental conditions are discussed below:

- Thermal $N_2O$ decomposition.

In order to study the importance of thermal $N_2O$ decomposition, 1500 ppm $N_2O$ has been suplied to the empty reactor in the temperature range of 600 to 1000 °C.

- $N_2O$ reduction reaction at the char surface area.

During these experiments a gas mixture of $N_2O$ in $N_2$ (inert atmosphere) was fed through a fixed bed consisting of 45 g of El-Cerrejon char in order to study the reaction rate and the reaction order. Table 6.3.2 shows the experimental conditions.

Table 6.3.2. Experimental conditions.

| | |
|---|---|
| Bed temperature | From 773 to 1023 K |
| Concentration $N_2O$ inlet in $N_2$ | 1200 and 130 ppmV |
| Mean char diameter | 1 and 1.5 mm |

- $N_2O$ formation through NO reduction at the char surface area.

From literature it is not clear whether this $N_2O$ formation mechanism plays a significant role. To study this mechanism a mixture of 450 ppmV NO in nitrogen was fed through the reactor containing a fixed bed of 45 g of El-Cerrejon char. Table 6.3.3 gives the experimental conditions.

Table 6.3.3. Experimental conditions.

| | |
|---|---|
| Bed temperature | From 773 to 1073 K |
| Mean char diameter | 1 and 1.5 mm |

- Micro-scale combustion experiments.

Micro-scale combustion experiments (oxygen atmosphere) have been conducted to study the influence of temperature and particle diameter the $N_2O$ and NO emissions. Table 6.3.4 shows the experimental conditions.

Table 6.3.4. Experimental conditions.

**Constant process conditions:**

| | | |
|---|---|---|
| Fluidizing velocity | 0.4 | [m/s] |
| Bed height (static) | 0.1 | [m] |
| Bed height (expan.) | 0.15 | [m] |
| Diameter bedmaterial | 0.6 - 0.8 | [mm] |
| Air ratio | 1.2 | [-] |
| Char supply | 0.3 | [kg/hr] |

**Experimental variations:**

| | |
|---|---|
| Bed temperature | From 1023 to 1173 K |
| Sieve fraction char | 1-2 and 2-3 mm |

## 6.3.4.4. EXPERIMENTAL RESULTS

In this chapter the results from the experimental program will be reported.

### *6.3.4.4.1 Thermal $N_2O$ decomposition*

Figure 6.3.6 shows the $N_2O$ conversion in relation with temperature. It can be seen that the thermal $N_2O$ decomposition is not important below reactor temperatures of 900 °C. However, it is not clear whether this reduction is purely thermal, because the stainless steel gas sampling tube in the reactor can also have a catalytic effect on the $N_2O$ reduction reaction.

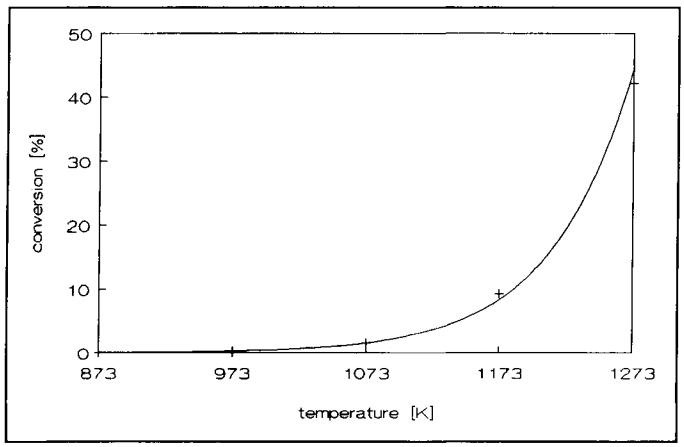


Figure 6.3.6. Conversion in relation to temperature for thermal $N_2O$ decomposition.

### *6.3.4.4.2 $N_2O$ reduction reaction on the char surface area*

From experimental data the reaction rate and the order m of the reaction has been derived taking into account the effects of external and internal mass transport limitations. The value of the effective diffusivity has been estimated to be $1 * 10^{-5}$ $m^2/s$.

Reaction order m = 1 appeared to be the best fit for the experimental data. Figure 6.3.7 shows a plot of the reaction rate constant calculated from experimental data in relation to the temperature for m = 1.

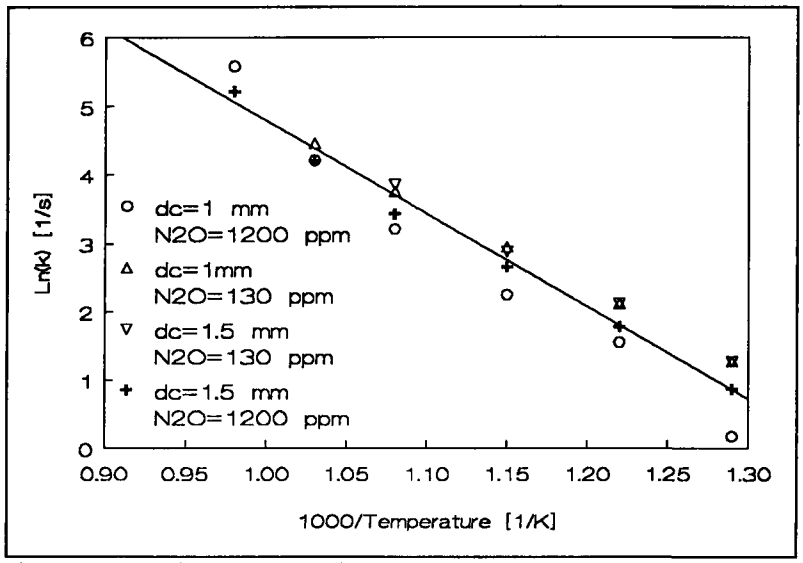


Figure 6.3.7. Reaction rate constant in relation to temperature.

The reaction rate constant for the $N_2O$ reduction reaction on the char surface area can be written as follows:

$$k_{N_2O} = 9.16 * 10^7 \, EXP\left(\frac{-13540}{T}\right) \left[\frac{1}{s}\right] \tag{6.3.29}$$

*6.3.4.4.3 $N_2O$ formation through NO reduction on the char surface area*

During these experiments no $N_2O$ formation from NO could be detected. From the data obtained during these experiments a first order behaviour was found for the NO reduction reaction on the char surface area. The following reaction rate was found:

$$k_{NO} = 2 * 10^8 \, EXP\left(\frac{-14800}{T}\right) \left[\frac{1}{s}\right] \tag{6.3.30}$$

*6.3.4.4.4 Combustion experiments*

Figures 6.3.8 and 6.3.9 show the concentrations of $N_2O$ and NO measured during micro-scale combustion experiments.

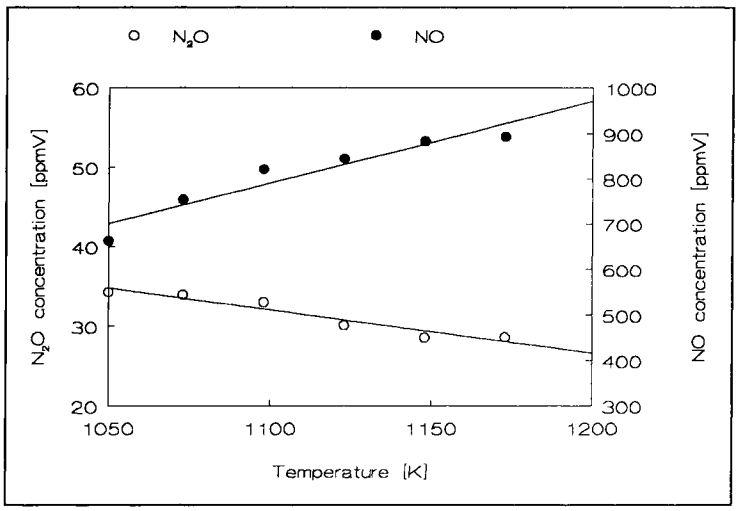


Figure 6.3.8. Overall $N_2O$ and NO concentrations, $d_{char}$ = 1 -2 mm.

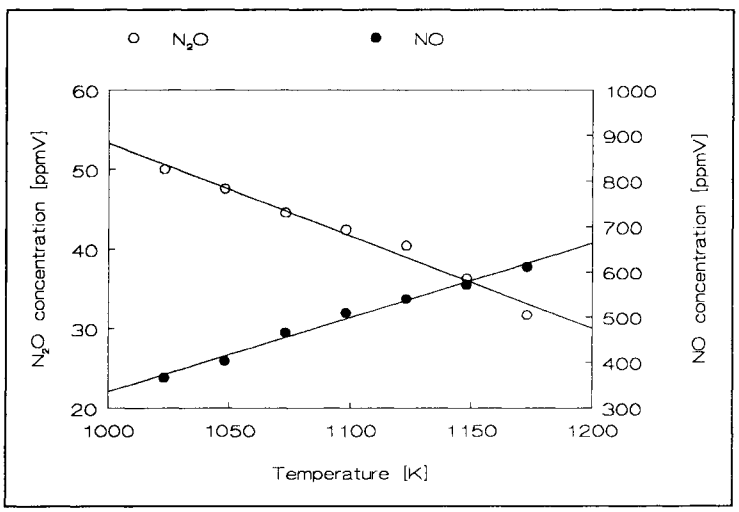


Figure 6.3.9. $N_2O$ and NO concentrations, $d_{char}$ = 2 - 3 mm.

From figures 6.3.8 and 6.3.9 it can be seen that the NO concentration increases with increasing temperatures and that the $N_2O$ concentration decreases with increasing temperatures. Futhermore it can be seen that the NO concentration increases while the $N_2O$ emission decreases when burning smaller char particles.

*6.3.4.4.5 Model results*

A computer program has been written to simulate the micro-scale experiments. The reactor is modeled as a plugflow reactor. Earlier experiment have shown that the char is homogeneously mixed in the bed and that the reactor shows a one fase behaviour. The $N_2O$ and NO reduction capacities of a single char particle ( formulas (6.3.23) and (6.3.26)) have been used. The first order reaction rate constant in oxygen for the burning of the char has been adopted from Smith [15]:

$$k_{char} = 20.85 * T * EXP\left(\frac{-21600}{T}\right) \left[\frac{m}{s}\right] \tag{6.3.31}$$

All model parameters are known except for the primary formation rate of char-N to $N_2O$ ($= \gamma_{N2O}$) and char-N to NO ($= \gamma_{NO}$). Experimental data will be used to get values for $\gamma_{N2O}$ and $\gamma_{NO}$ (see fig. 6.3.10). These factors must physically satisfy the following expression:

$$2\gamma_{N_2O} + \gamma_{NO} \leq 1 \tag{6.3.32}$$

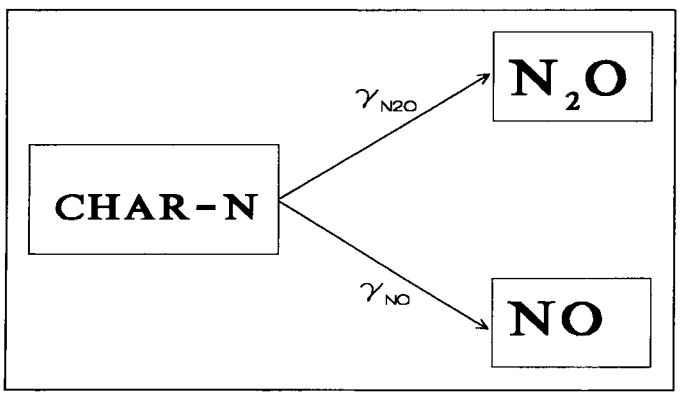


Figure 6.3.10. Meaning factors $\gamma_{N2O}$ and $\gamma_{NO}$.

Figures 6.3.11 and 6.3.12 show the results of the calculations. Figure 6.3.11 shows $\gamma_{N2O}$ in relation to temperature and particle diameter. Figure 6.3.12 shows $\gamma_{NO}$ in relation to temperature and particle diameter. In figure 6.3.13 the summation of the latter two ($2*\gamma_{N2O} + \gamma_{NO}$) is shown.

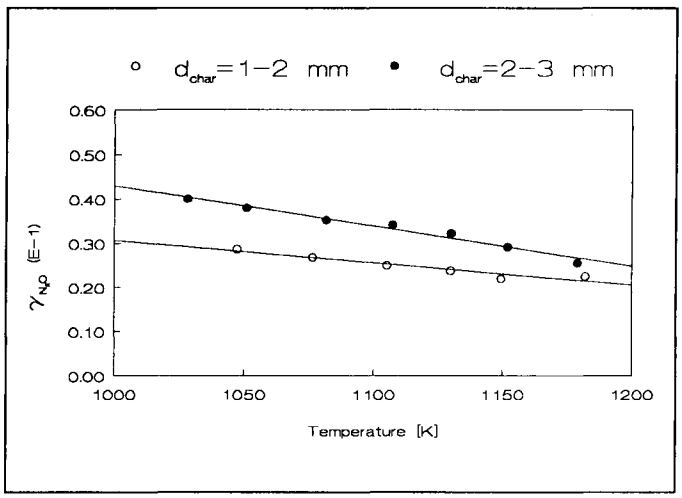


Figure 6.3.11. $\gamma_{N2O}$ in relation to temperature and particle diameter.

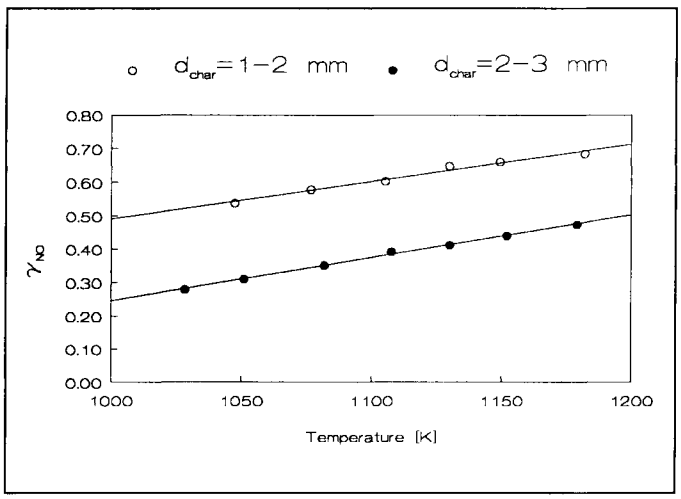


Figure 6.3.12. $\gamma_{NO}$ in relation to temperature and particle diameter.

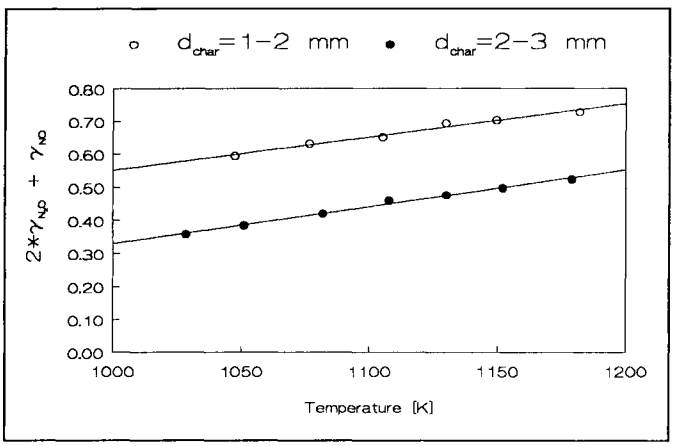


Figure 6.3.13. $2*\gamma_{N2O} + \gamma_{NO}$ in relation to temperature and diameter.

From fig. 6.3.11 the conclusion can be drawn that the amount of char bound nitrogen converted into $N_2O$ decreases proportional with increasing temperature. It is also clear that the larger char particle diameter enhances the amount of $N_2O$ formed by direct oxidation of char bound nitrogen. Figure 6.3.12 shows that the amount of NO formed by direct oxidation of char bound nitrogen increases proportional with increasing temperature and decreases with increasing char particle diameter. Figure 6.3.13 shows that NO and $N_2O$ account for 35 to 75 % of the char bound nitrogen depending on temperature and particle diameter. It could be expected that the factors $\gamma_{N2O}$ and $\gamma_{NO}$ are dependent on the particle temperature. It was however unexpected that the above mentioned factors are a function of the particle size. An explanation for this could be the unknown value for the reaction rate constant for the combustion reaction $k_{char}$ which is adopted from literature.

## 6.3.5 CONCLUSIONS.

The main source of $N_2O$ and NO during char combustion in a fluidized bed reactor is the direct oxidation of char bound nitrogen. This $N_2O$ and NO can be reduced on the char surface area. For both reduction reaction a first order reaction behaviour in the gaseous component was found by fitting the reaction order to experimental data. No $N_2O$ formation could be detected by NO reduction on the char surface area.

Micro-scale char combustion experiments showed that the $N_2O$ concentration decreases proportional with increasing temperature while the NO concentration increases proportional with increasing temperature. These experiments also show that

the $N_2O$ concentration increases with larger particle diameters of the char. The NO concentration decreases with larger particle diameter.

Expressions for the $N_2O$ and NO reduction capacities for the so-called linear case have been used in a computer program to determine the factors $\gamma_{N2O}$ and $\gamma_{NO}$ which represent the primary formation of $N_2O$ and NO inside the char particle. These factors show a linear temperature dependence. Also an influence of the char diameter was found, which might be caused by an incorrect value for the reaction rate constant of the combustion reaction. From these factors it is clear that $N_2O$ and NO account for 35 to 75 % of the char bound nitrogen, depending on temperature and particle diameter.

The single particle model has been used to derive expressions for the $N_2O$ and NO reduction capacities of a single particle for the linear case. The latter means the assumption of constant internal surface area of the char and constant effective diffusivity. In reality both the internal surface area and the effective diffusivity will change because the char is involved in the combustion reaction leading to changes inside the particle. Further work must be done to expand the expressions for the reduction capacities for the non-linear case, as decribed in Brem [10] and to validate the model with experimental data. Also the $N_2O$ and NO reactions during volatile combustion should be included so the model can eventually be used to predict the $N_2O$ and NO emission from a fluidized bed combustor.

### 6.3.6 SYMBOLS

| | | |
|---|---|---|
| $A$ | surface area of the char | $m^2/g$ |
| $a$ | stoichiometric reaction coefficient | - |
| $A_g$ | reaction surface area per unit of volume | $m^2/m^3$ |
| $Bi_m$ | Biot number for mass transfer | - |
| $C$ | reduced oxygen concentration | - |
| $C_j$ | concentration of component j | $mol/m^3$ |
| $d$ | diameter | m |
| $D_e$ | effective diffusivity | $m^2/s$ |
| $F_c$ | carbon conversion | - |
| $k$ | reaction rate constant | 1/s, m/s |
| $m$ | reaction order | - |
| $N$ | reduced NO concentration | - |
| $N^*$ | reduced $N_2O$ concentration | - |
| $R$ | initial particle diameter | m |
| $r$ | particle diameter | m |
| $r$ | radial coordinate | m |
| $R_{NO}$ | NO reduction capacity of a single particle | - |
| $R_{N2O}$ | $N_2O$ reduction capacity of a single particle | - |
| $T$ | temperature | K |
| $t$ | time | s |
| $W_g$ | bulk density of the char | $kg/m^3$ |
| $X_j$ | mole fraction of component j | - |

| | | |
|---|---|---|
| $X_{NC}$ | molar ratio of nitrogen and carbon in the char | - |
| $\gamma_{NO}$ | molar ratio of the amount of $N_2O$ formed by direct oxidation from the total amount of nitrogen in the char | - |
| $\gamma_{N2O}$ | molar ratio of the amount of NO formed by direct oxidation from the total amount of nitrogen in the char | - |
| $\epsilon$ | fixed-bed porosity | - |
| $\theta$ | reduced time | - |
| $\zeta$ | reduced particle diameter | - |
| $\rho$ | density | $kg/m^3$ |
| $\phi$ | Thiele modulus | - |

Subscripts

| | |
|---|---|
| $_c$ | char |
| $_f$ | formation |
| $_{NO}$ | with respect to NO |
| $_{N2O}$ | with respect to $N_2O$ |
| $_o$ | with respect to $O_2$ |
| $_r$ | reduction |
| $_s$ | with respect to carbon |
| $_\infty$ | bulk |

## 6.3.7 REFERENCES.


1 Hulgaard, T. Nitrous oxide from combustion. Ph.D. Thesis, Technical University of Denmark, Denmark (1991).

2 Johnsson, J.E., Nitrous oxide formation and destruction in fluidized bed combustion - a literature review of kinetics. 23rd IEA-AFBC-Meeting. Firenze, (1991).

3 De Soete, G.G., Heterogeneous $N_2O$ and NO formation from bound nitrogen atoms during char combustion. Twenty-third Symposium (international) on combustion.

4 Wojtowicz, M.A., Oude Lohuis, J.A., Tromp, P.J.J., Moulijn, J.A. $N_2O$ formation in fluidized bed combustion of coal. Eleventh International Conference of Fluidized Bed Combustion. ASME, New York, p.1013-1020, (1991).

5 Bramer, E.A., Valk, M. Nitrous oxide and nitric oxide emissions by fluidized bed combustion. Eleventh International Conference on Fluidized Bed Combustion, ASME, New York, p.701-708, (1991).

6 De Soete, G.G., Formation of nitrous oxide from NO and $SO_2$ during solid fuel combustion. Proceedings of 1989 Joint Symposium on Stationary Combustion $NO_x$ Control, San Francisco, (1989).

7 Amand, L.E., Andersson, S. Emissions of nitrous oxide ($N_2O$) from fluidized bed boilers. The Tenth International Conference on Fluidized Bed Combustion. ASME, New York, (1989).

8 Lisa, K., Santala, P., Hupa, M. Formation of nitrous oxide from ammonia on lime surfaces. Abo Akademi, Finland, Report no. 90-50, (1990).

9 De Soete, G.G. Heterogeneous reactions on coal and char, with emphasis on $N_2O$ formation. Conference held at Chalmers, Goteborg, Sweden, (1988).

10 Santala, P., Lisa, K., Hupa, M. Catalytic destruction of $N_2O$ in a fixed bed laboratory reactor, Abo Akademi, Finland, Report no. 90-6, p.1-22, (1990).

11 Miettinen, H., Stromberg, D., Lindquist, O. The influence of some oxide and sulphate surfaces on $N_2O$ decomposition. Eleventh International Conference on Fluidized Bed Combustion, ASME,

New York, p.999-1004, (1991).
12 Brem, G. Mathematical modeling of coal conversion processes. Ph.D. Thesis, Twente University of Technology, Enschede, Thew Netherlands, (1990).
13 Ishida, M., Wen, C.Y. Comparison of kinetics and diffusional models for solid-gas reactions. AIChE Journal, vol. 2, (1988).
14 Engelen van, A.B., Honing van der, G. Coal characterization by combustion experiments in a small scale fluidized bed, interpreted by an analytical single porous particle conversion model, Twente University of Technology, Enschede, The Netherlands, (1990).
15 Smith, I.W. The intrinsic reactivity of carbon to oxigen. Fuel, vol. 57, p.303-314, (1978).